BNL-228873-2025-JAAM

Grazing Incidence Wide-Angle X-ray Scattering of Water Adsorption in Polyamide Barrier Layers of Reverse Osmosis Membranes

Q. Fu, B. Ocko

To be published in "Macromolecules"

February 2025

Photon Sciences

Brookhaven National Laboratory

U.S. Department of Energy

USDOE Office of Science (SC), Basic Energy Sciences (BES). Scientific User Facilities (SUF)

DISCLAIMER

Grazing Incidence Wide-Angle X-ray Scattering of Water Adsorption in Polyamide Barrier Layers of Reverse Osmosis Membranes

Qinyi Fu[1], Size Zheng[1], Nisha Verma[1], Roberto Gambarini[2], Tao Wei[2,3,*], Benjamin M. Ocko[4,*] and Benjamin S. Hsiao[1,*]

[1] Department of Chemistry, Stony Brook University, Stony Brook, NY 11794, United States

[2] Department of Chemical Engineering, University of South Carolina, Columbia, SC 29208 United States

[3] Department of Biomedical Engineering, University of South Carolina, Columbia, SC 29208, United States

[4] National Synchrotron Light Source II, Brookhaven National Laboratory, Upton, NY 11973, United States

*Corresponding Authors

Email: taow@mailbox.sc.edu, ocko@bnl.gov, benjamin.hsiao@stonybrook.edu

For Table of Contents use only

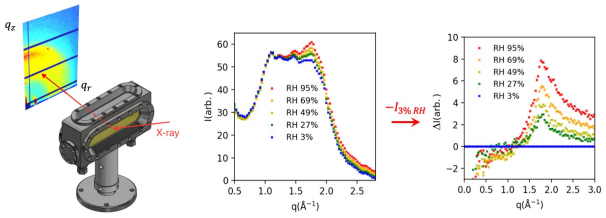

Abstract

To understand the relationship between the intermolecular structure of aromatic polyamide (PA) scaffold and its water adsorption capability in the barrier layers of reverse osmosis (RO) membranes, a grazing incidence wide-angle X-ray scattering (GIWAXS) study was carried out on freestanding PA thin films at varying relative humidity (RH) conditions. The scattering results were analyzed by an Interface Scattering Model, containing a phase factor between a PA chain and an adsorbed water molecule. This model yielded good fits to the GIWAXS profiles where the water adsorption was found to vary linearly with RH. Atomistic molecular dynamics (MD) simulations were also performed to complement the experimental study. The simulations revealed that a rapid condensation layer initially formed on the PA film surface, followed by the slow water molecule diffusion inside the PA membrane. Sparse adsorbed water, isolated in sub-nanopores of the PA film adjacent to the polar atoms, even in very low quantities, enhances the X-ray scattering. Atomistic simulations at the microscopic scale provide partial support for several X-ray scattering findings.

Keyword

GIWAXS, Atomistic MD simulations, RO membranes, Polyamide structure, Water adsorption.

Introduction

Among the various types of reverse osmosis (RO) membranes, cross-linked aromatic polyamide (PA) thin-film composite (TFC) membrane provides the most effective desalination performance.[1] A typical TFC RO membrane consists of three layers: a top PA barrier layer with densely cross-linked structure which is solely responsible for salt rejection (the layer thickness is between 50 and 300 nm), a polysulfone mid-layer to support the PA barrier layer, and a nonwoven substrate to provide the overall mechanical strength.[2] The use of interfacial polymerization (IP) methods to prepare the PA barrier layer with no heat curing or surfactant addition was first demonstrated by Cadotte et al. in the 1970s.[3] The interfacial polymerized TFC RO membranes exhibit a good balance of permeability and permselectivity due to their self-sealing and self-terminating properties in the film growth process.[4] The progressive achievements to fine tune the structure and property relationship to fabricate TFC RO membranes have enabled their widespread use in desalination processes.[5] Researchers have systematically optimized the barrier layer properties by using different monomers, adding surfactants and additives, adjusting reaction conditions and alternating the substrates, in order to optimize the membrane performance with high permeability while maintaining good selectivity and rejection ratio.[1] Currently, high performance commercial RO membranes can achieve a salt rejection ratio larger than 99.8% to produce freshwater from sea water with an energy consumption below 2 kWh/m.[3, 6] However, these membranes are still prone to fouling and chlorine attacks, which have become a major research focus area in many laboratories.[7]

In typical IP process to fabricate the PA barrier layer, a microporous substrate is first soaked with the m-phenylenediamine (MPD) solution in water, and then exposed to a solution of 1,3,5-benzenetricarbonyl trichloride (TMC) in hexane. Through polycondensation, a partially cross-linked PA scaffold is formed.[6, 8] Essentially, three conditions should be met inside the PA layer to achieve desired permeability and rejection ratio: sufficient free volume, appropriate pore size distribution, and sufficient affinity with water molecules.[9-10] The structure of the PA layer can be further modified by using different monomers, monomer concentrations, solvent type, reaction time, and curing conditions.[11] Although researchers have invested a great deal of effort to optimize the properties, there are knowledge gaps required for a detailed understanding of molecular scale structure and property relationship. Conventional characterization methods, such as scanning electron microscopy (SEM),[5, 12-13] atomic force microscopy (AFM),[14-15] Fourier-transform infrared spectroscopy (FTIR),[14, 16-17] and positron annihilation spectroscopy (PALS),[18-20] are insufficient to fully reveal the mechanism of how water molecules transport in the PA networks. In our view, an improved understanding of the structure-performance relationships not only has the potential to enable a significant advance in the membrane science relevant to desalination, but also for other small molecule separations (e.g., gas separation).

The techniques of X-ray scattering, such as small-angle X-ray scattering (SAXS) and wide-angle X-ray scattering (WAXS), are powerful tools to directly investigate the structure, size, and shape of polymer scaffolds.[21-22] Generally, SAXS can deliver structural information of polymers between 2-200 nm in size, while WAXS can resolve atomic and molecular spacings at the sub-nm scale.[23] The focus of this research is to use the grazing-incidence WAXS (GIWAXS) to investigate the intermolecular packing structure of the PA barrier layer at the atomic level in the presence of

varying water content (relative humidity) and under varying solvent activation conditions. In the past, a few papers have reported using the WAXS method to study the molecular structure of the PA barrier layer in RO membranes. For example, Singh et al. performed WAXS experiments on bulk PA samples prepared at the organic/water interface, which revealed a mean molecular spacing of 5.1-5.3 Å (peak position at around 1.2 $Å^{-1}$) due to the intra-chain molecular packing.[24] Matthews later also prepared bulk PA samples using the same monomer concentrations as in Singh's study (i.e., 2 wt.% MPD and 0.1 wt.% TMC) and measured its structure with WAXS.[25] In contrast to Singh's results, Matthews observed a scattering peak centered at 1.34 $Å^{-1}$, where the discrepancies were explained by differences in sample preparation. Although these studies have revealed information regarding the molecular spacings of PA materials, they were limited in scope with no detailed understanding of the structural origin of the results. Additionally, neutron scattering studies were also carried out to study PA samples. Small-angle neutron scattering (SANS) and grazing-incidence small-angle neutron scattering (GISANS) studies using the neutron contrast provided by D_2O have yielded complementary structural information from X-ray scattering and revealed the pore structure in PA films. For example, Pipich et al. used both SANS and PALS techniques to evaluate the average size of pores in freestanding PA films prepared at the hexane/water interface using the same monomer concentrations as reported by Singh,[24] where the average diameter of pores was found to be about 6 Å.[26] Furthermore, using supercritical CO_2 at elevated pressures, their SANS study revealed a network of interconnected pores approximately 16 Å in size with a fractal structure.[26] Other experimental studies[19] and molecular simulations work[27] also reported the similar results. To yield new insights into this topic, we have used GIWAXS to characterize freestanding PA films under a dry vacuum condition.[28-29] Unfortunately, the GIWAXS results could not directly reveal the average pore size in these films. Atomistic

molecular dynamics (MD) simulations by Wei et al. argued the pores with dimensions of 4-5 Å are formed due to the existence of two different aromatic packing motifs in the PA scaffold: T-shaped and parallelly stacked aromatic packing motifs,[30-32] where these pores play a crucial role in water-salt separation.[30] This hypothesis has not been fully vetted, and directed experimental studies are required. Our GIWAXS measurements did not show a signal for larger pores with a dimension of 16 Å (i.e., $q = 0.39$ Å^{-1}).

PA film's water swelling and expansion behavior at varying relative humidity (RH) has been measured by the X-ray reflectivity (XR) method. For example, Karan et al. reported a swelling ratio of ~ 8% in thin PA films (~ 20 nm thickness) from dry to wet state.[33] Chan et al. concluded that such swelling is caused by the thermodynamic balance between the enthalpic driving force from PA/water mixing and the resistance to PA chain expansion.[34] They used the Painter-Shenoy model and obtained reasonable fits for the swelling results from PA films at varying humidity and further estimated the number of PA repeating units between the crosslinking conjunctions. In our previous X-ray reflectivity work, we also observed the reversible swelling processes (~ 5% expansion in thickness) in freestanding PA films (also ~ 20 nm thickness) in going from 0% RH to 100% RH.[28] A goal of the present study is to understand the interplay between the water molecules and the PA scaffold. To understand this relationship, we have carried out GIWAXS studies of freestanding PA thin films at varying RH conditions and under different solvent activation treatments. To analyze the GIWAXS data, we developed an Interface Scattering Model to address the issue of water adsorption. Additionally, we conducted atomistic molecular dynamics (MD) simulations, in part to investigate how water adsorption modifies the X-ray scattering profiles. Atomistic MD simulations offer new insights into atomic-scale information as

well as dynamics across timescales ranging from sub-nanoseconds to microseconds. It has the potential to enhance our understanding of interfacial hydration in IP materials and to aid in the development of new membrane materials.[35-36]

Experimental

Materials and Sample Preparation

In this study, 1,3,5-benzenetricarbonyl trichloride (TMC, 98.0+%) was purchased from TCI America, Oregon, USA, m-phenylenediamine (MPD, 99+%) was purchased from Acros Organics, Massachusetts, USA.

The sample preparation procedure for freestanding PA films by interfacial polymerization (IP) is as follows. A polished silicon wafer was placed at the bottom of a 50 mL beaker, followed by adding an MPD aqueous solution and then a hexane buffer layer (~ 2 mm thick). The interfacial polymerization was carried out by drop-wise addition of a TMC/hexane solution. With a hexane buffer layer, MPD monomers would slowly diffuse into the hexane phase and react with TMC monomers to produce a homogenous and smooth PA film. In our experiment, we used a 0.1 wt% MPD aqueous solution and 0.04 wt% TMC/hexane solution to carry out interfacial polymerization. After 60 min of IP, the unreacted solution was slowly drained with a syringe pump, leaving behind a very thin PA film (~ 20 nm thickness) on the silicon substrate. Afterwards, a post-treatment step

was performed using a 1.0 wt% solution of citric acid to remove unreacted MPD monomers. After waiting for 20 min, the beaker was drained. The beaker was refilled with deionized water to rinse the sample, and then drained again after 60 min. Finally, the PA film deposited on the Si substrate was dried at room temperature in a desiccator.

Grazing Incidence Wide-Angle X-ray Scattering (GIWAXS) Characterization

GIWAXS experiments on the freestanding PA films were carried out at the 11-BM Complex Materials Scattering (CMS) beamline in the National Synchrotron Light Source II (NSLS-II), Brookhaven National Laboratory (BNL). The GIWAXS experiments were conducted at the energy of 13.5 keV (or 0.918 Å wavelength), where the sample chamber and the detector were placed in a vacuum chamber to reduce the background scattering. The monochromatic X-ray beam impinged on the PA film sample supported on a silicon wafer at an incident angle a_i, where the beam was scattered under the exit angle of a_f and the out-of-plane angle of ϕ. Both were captured by an area detector (Pilatus 800K, DECTRIS, Pennsylvania, USA). In our measurements, the chosen incident angle $a_i = 0.12°$ was slightly larger than the incident angle of the silicon substrate. This arrangement allowed the incident beam to penetrate the full thickness of the entire PA layer. The q range of the GIWAXS setup was from 0.1 $Å^{-1}$ to 5 $Å^{-1}$, relevant to probing the molecular packings of the PA molecules.

The effect of humidity on the structure changes in PA films was carried out using a custom-designed, GIWAXS humidity cell (Figure 1). This cell was capable of holding eight samples simultaneously. To reduce background, the sealed humidity cell was placed in the CMS vacuum chamber and evacuated, leaving the environmental cell at about an overpressure of 1 atm. The relative humidity (RH) was monitored by a humidity sensor inside the humidity cell and controlled through the mixing of wet (via a bubbler) and dry nitrogen gas streams, where both flow rates could be adjusted remotely, and the tubes carrying the humid streams were passed through the CMS vacuum to the environmental chamber. In the humidity study, the GIWAXS signals were first monitored over a sufficiently long time to determine the suitable time for PA films to reach equilibrium under each RH condition. These studies showed that the system could be stabilized within 10 min after the RH value changed from 95% to 65%. Considering an ~20 nm PA film thickness, it is likely that the 10 min corresponded to the system response time rather than the time required for PA to reach a thermodynamic equilibrium through diffusion. In our studies, the system was equilibrated for 20 min after each humidity change before collecting the scattering data. At the start of each "humidity run", the PA films were stabilized at 95% RH, and the surface normal was aligned with X-ray beam to set the incident angle. After acquiring X-ray data at 95% RH, the RH was reduced to 69%, 49%, 27%, and 3%, where additional X-ray data was obtained. To observe the reversibility of the scattering results, the RH was again equilibrated at 95%, where additional X-ray data was acquired.

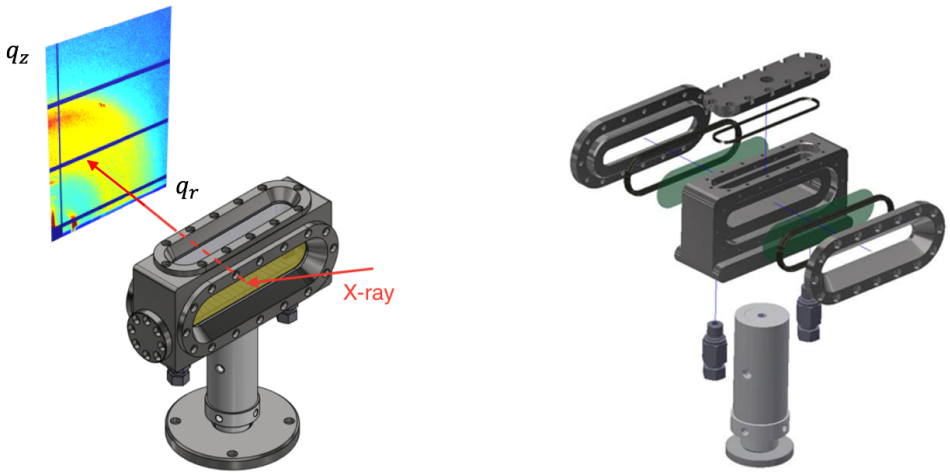

Figure 1. Humidity cell designed for GIWAXS measurements carried out at the CMS beamline in NSLS II, BNL. Left: assembled cell; Right: essential cell components.

In the humidity study, the scattering background change at different RH was first considered. Specifically, X-ray absorption by the air/water vapors in the custom-designed humidity cell was evaluated. The X-ray path length of the humidity cell was estimated to be 3 cm. According to our calculation, the absorption from air/water vapors inside the custom-designed humidity cell was less than 0.6% of the direct beam at the photon energy level of 13.5 keV. As a result, the water vapor induced scattering background change was neglected in the data analysis.

Atomistic Molecular Dynamics Simulations

Molecular dynamics (MD) simulations were performed to investigate the effects of water on the X-ray scattering signals from PA thin films and the water diffusion process during adsorption. A dry model of PA thin film having a degree of crosslinking around 70% between MPD and TMC was used. Here the degree of crosslinking is defined as the percentage of fully reacted TMC molecules, where all three acyl chloride groups have reacted with MPD monomers, relative to the initial total number of TMC molecules in the system.[31-32] This film was constructed in our previous work by using a simulation box with dimensions of 90 × 90 × 150 $Å^3$.[32] Periodic boundary conditions were applied in the X-, Y-, and Z-axes. In this study, due to the microscopic dimensions of the simulation box, it was not practical to scale it directly to match the experimental RH. This is because with such a small simulation scale, even under conditions equivalent to 95% RH in the macroscopic scale, the number of water molecules present in the simulated system would be very low (approaching zero). Without losing generality, it was assumed that the water molecules in the gas phase would eventually accumulate on the surface of PA film during adsorption due to water-surface and water-water interactions. As a result, 720 water molecules were randomly added into the vacuum space at the top and bottom of the simulation box. This condition was approximately 1000 times higher than the saturated vapor density. To validate the simulation results, we also performed another simulation using only 50 water molecules, and the concentration of this new system was only 7% of that in the system containing 720 water molecules. In the end, both systems showed a similar process: an initial rapid condensation of water molecules on the membrane surface, followed by prolonged diffusion through the membrane interior (Figures S1 and S2 in *Supporting Information*).

In this simulation, the CHARMM36 force field was employed to construct the PA thin film, where the TIP3P water model was utilized to represent the water molecules.[37-38] Additionally, the particle mesh Ewald (PME) method was applied to calculate the long-range electrostatic interactions.[39] The simulation time step was set to 1.0 fs, and a total of 300 ns production run was performed under the NVT ensemble. The system temperature was maintained at 298 K using the V-rescale thermostat.[40] The analyses were conducted on the last 20 ns of the production run. All simulations were carried out using the GROMACS 2022.2 software.[41]

Results and Discussion

GIWAXS Study of Freestanding PA Films under Varying Humidity

Figure 2A shows the 2D GIWAXS pattern of the PA film at 95% RH. This pattern contained the scattering signals from the PA film, the background scattering from the Kapton window, and the air and moisture in the humidity cell. As previously observed, the pattern showed a higher scattered intensity along the q_z direction, indicating the existence of orientational anisotropy. This aligns with our earlier studies on dry freestanding PA films, which revealed two scattering peaks, each with distinct azimuthal orientations.[28] There, we attributed this to two different aromatic packing motifs—parallel and perpendicular—with surface-induced preferential orientation. In general, the molecular spacing is closer packed for orientations along the surface normal direction than that along the direction in-plane of the surface.[29] To investigate the average profiles, circular averaging of the linear profiles at different azimuthal angles (χ) along the q-axis

was carried out (Figure 2B). We note that this average emphasizes the scattering along the surface normal direction because the scattering is stronger along this direction. Figure 2B shows the evolution of the circularly averaged profiles as the RH varied from 3% to 95%. Unlike the GIWAXS profiles of the PA films collected under vacuum, the profiles obtained from the PA films inside the humidity cell showed peaks and features emerging in the low-q region (~ 1 Å^{-1}) due to Kapton scattering (the minor scattering from water vapor was ignored as discussed earlier). The intensity upturn below 0.5 Å^{-1} in Figure 2B has been observed by small-angle scattering studies,[24,26] which was attributed to pore scattering but our results do not allow us to make this claim. It is interesting to note that while the scattering profiles at different RH values showed a close agreement at low q (< 1 Å^{-1}), the scattered intensity at q ~ 1.85 Å^{-1} was found to increase noticeably with increasing RH.

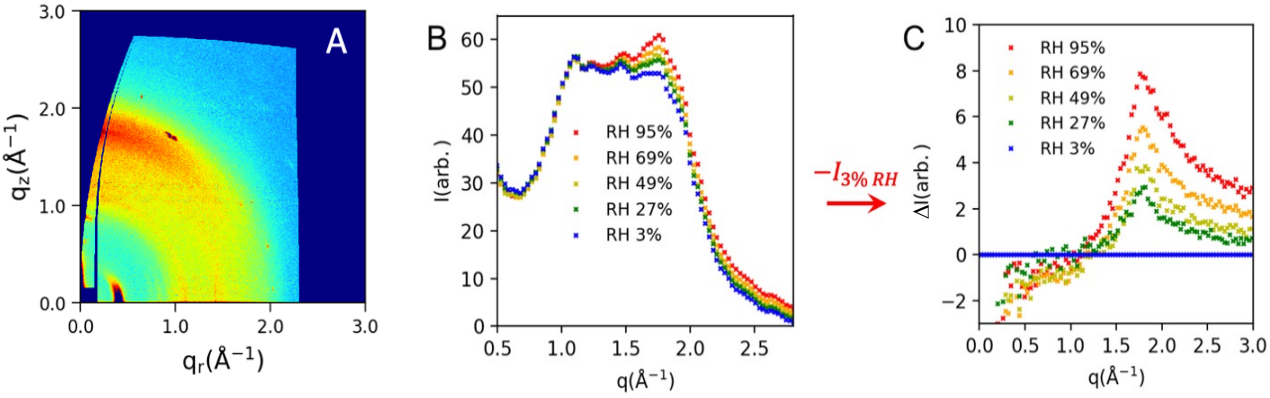

Figure 2. GIWAXS patterns of a freestanding PA film. (A) The scattering pattern obtained at 95% RH using a humidity cell. (B) Evolution of circularly averaged intensity profiles from scattering patterns at varying RH levels. (C) Evolution of circularly averaged profiles at varying RH levels, after subtracting the profile at 3% RH.

To quantify the background scattering, data was collected by moving the humidity cell down by 1 mm, such that the X-ray beam did not impinge on the PA sample. However, it is not straightforward to use this result in the analysis, since it provides the background intensity from the direct beam impinging on two windows, and we don't know the reflected flux impinging on the second window. Rather, we calculated and analyzed the differences of the signals by subtracting the intensities of the 3% RH. The results are shown in Figure 2C.

In Figure 2C, the intensity differences from subtracting the results at 3% RH provide insight into the effects of humidity. It was seen that in the low q region (< 1 $Å^{-1}$), the scattering profiles went negative with increasing RH. In contrast, in the high q region (> 1.5 $Å^{-1}$), the scattering peak became more enhanced with increasing RH. These intensity variations cannot be explained by the scattering from bulk water as water exhibits broad scattering features peaked at 2.0 $Å^{-1}$, 2.85 $Å^{-1}$ and 4.5 $Å^{-1}$.[42] As the effect of X-ray absorption from the adsorbed water molecules in the gas phase is ~ 0.01%, hence it does not contribute to the observed behavior. Further, the small amount of water in the film should not contribute to absorption. Thus, we hypothesize that the negative intensity in the low q region is because the scattering phase factor between the adsorbed water and the polymer chain is close to π, giving rise to destructive interference, hence the scattered intensity decreases. In contrast, the increase in intensity observed at the higher q values would result from constructive interference with the polymer chains at the higher RH. This hypothesis will be further discussed in the context of the MD simulations.

Interface Scattering Model for Data Analysis

Based on the experimental findings presented above, we propose an Interface Scattering Model (ISM) to describe the humidity-dependent scattering change in Figure 2C. This phenomenological model incorporates a phase factor between the absorbed water molecules and the polymer chains, and accounts for both the decrease and increase in the scattered intensities observed at different q values. Before describing the model, we first present the ISM for a dry sample (i.e., in vacuum without water moisture), which can be reduced to the Lorentzian model used previously.[28] First, we propose that the scattered intensity (in vacuum) is given by:

$$I_{\text{vacuum}}(q) = I\left|\frac{1}{i+\frac{q-q_1}{\Delta_1}}+\frac{r\cdot e^{i\phi}}{i+\frac{q-q_2}{\Delta_2}}\right|^2 + I_B \qquad (1)$$

where ϕ is a phase factor between the two independent scattering terms (term *1* and term *2*), q_1 and q_2 are the peak positions of the two terms, $\Delta_1$and Δ_2 are the corresponding q-widths, I is an overall intensity factor, r is a ratio between the scattered intensities from two terms (I_1 and I_2), and I_B represents the linear sloping background. If ϕ = 90°, there is no correlation between the two scattering terms as the two cross-terms cancel each other, hence Eq. (1) becomes the sum of two Lorentzian terms having the expression as follows:

$$I_{\text{vacuum}}(q) = \frac{I_1}{1+\left(\frac{q-q_1}{\Delta_1}\right)^2}+\frac{I_2}{1+\left(\frac{q-q_2}{\Delta_1}\right)^2} + I_B \qquad (2)$$

Eq. (2) resembles the fitting model containing two Lorentzian functions that we used in our previous study.[28] In a simple molecular system, the peak of each Lorentzian in q-space corresponds to the inverse ($2\pi/q$) of the characteristic molecular spacing. In our previous studies, the two fitted

Lorentzian peaks (positions correspond to molecular spacings of 4.0 and 3.5 Å, respectively) for the dry PA sample in vacuum are consistent with two different possible forms of parallel, "π–π" stacking of the aromatic cores and not from the intrinsic spacing of water channels.[28] These spacings may also represent the distance corresponding to moieties on the same polymer backbone and it is difficult to conclude with certainty the origin of these features. The results in the previous studies only exhibited a single peak with an asymmetric profile in the scattering profile.[28,29] We note that it is not possible to directly observe two distinct peaks (with molecular spacings of 4.0 and 3.5 Å) when their positions are too close to each other relative to their widths. However, the existence of two peaks can certainly explain the asymmetric scattering profile.

To model the humidity-dependent scattering changes, we first fitted the background subtracted GIWAXS profile from the dry PA film under vacuum using Eq. (1) where the result is shown in Figure S3 (*Supporting Information*). It was found that the fitted value of the phase factor ϕ for this film was 86°, while q_1 and q_2 were equal to 1.55 Å^{-1} and 1.85 Å^{-1}, respectively. As the fitted ϕ value was close to 90°, it suggests that there was no correlation between the two independent parts of the PA chain. In the subsequent analysis, we fixed ϕ = 90° and used the best fit values of q_1 = 1.55 Å^{-1}, q_2 = 1.85 Å^{-1} , Δ_1 = 0.27 Å^{-1}, Δ_2 = 0.38 Å^{-1}, and r = 1.64. To analyze the GIWAXS results from Figure 2C, we modeled the intensity difference between the wet and dry PA film at varying RH values. Using the ISM approach, we incorporated the effects of the adsorbed water through a humidity dependent, phenomenological amplitude term B and a phase factor e^{idq}:

$$\Delta I_{\text{humidity}}(q) = I\left(\left|B \cdot e^{idq} + \frac{1}{i + \frac{q-q_1}{\Delta_1}} + \frac{r \cdot e^{i\phi}}{i + \frac{q-q_2}{\Delta_2}}\right|^2 - \left|\frac{1}{i + \frac{q-q_1}{\Delta_1}} + \frac{r \cdot e^{i\phi}}{i + \frac{q-q_2}{\Delta_2}}\right|^2\right) \quad (3)$$

where d represents an effective distance between the water molecules and the PA chain. Here it is assumed that the background is humidity independent, and the form factor *B* of the water molecule is a constant over the range of interest in GIWAXS. For the other parameters ($q_1, q_2, \Delta_1, \Delta_2$, and ϕ), their values are the same as in Eq. (1), and thus are fixed in Eq. (3). In this equation, the first term $\left|B \cdot e^{idq} + \frac{1}{i+(q-q_1)/\Delta_1} + \frac{r \cdot e^{i\phi}}{i+(q-q_2)/\Delta_2}\right|^2$ represents the scattered intensity of the wet PA film obtained at the different RH levels, while the second term $\left|\frac{1}{i+(q-q_1)/\Delta_1} + \frac{r \cdot e^{i\phi}}{i+(q-q_2)/\Delta_2}\right|$ represents the scattered intensity of the dry PA film (in our case at 3% RH). These two terms were subtracted in the ISM model as required to match our data subtraction approach. During the profile fitting, we varied the two new parameters, *B* and *d*, along with *I* since the other parameters *I,* $q_1, q_2, \Delta_1, \Delta_2$, *r* and ϕ are pre-determined by fitting the GIWAXS profile of the same dry PA film (see above). Due to the simple nature of the present phenomenological model, we have not included a form factor for the water term. The GIWAXS profiles acquired at different RH values were fitted together, each with a different *B* value, but their phase factor *d* was restrained to a common value that fits all the data.

The analysis of the circularly averaged GIWAXS profiles at different RH values (Figure 2C) was carried out by using Eq. (3), where only *B*, *d* and *I* are varied for the data at each RH. In our analysis, we found the obtained *d* values were all close to zero for the tested film at different RH values. The physical meaning of *d* relates to the distance between water and the adsorption

site. However, the present model is an over-simplified case, since a range of d would be expected to account for multiple adsorption sites. The latter is evident by MD simulations (results to be discussed later), which show that the water molecules are often assembled in the vicinity of the hydrophilic side groups (i.e., carboxylic acid and amine groups) of the PA chain and not at a single site. Including such a range of adsorption sites would add much complexity to the ISM model and the data analysis would not be able to support so many new parameters. Furthermore, the phase factor d was set to zero in the subsequent analysis, since a small value of d always provided the best fits (we caution that the small d value might be an artifact of the over-simplified single-absorption site model).

The above fitting approach allowed the parameters B and I to vary at each RH, where the overall shape of the scattering profiles comes from the other parameters that were fixed. Figure 3 shows the best fits to the different scattering profiles using the ISM model. This approach is very appealing because this simple model *is capable of capturing the essential features of the profiles*. Specifically, the fits correctly exhibit the negative intensity differences in the low q regions (< 1 $Å^{-1}$) and the positive scattering peaks centered at ~1.85 $Å^{-1}$. From the analysis, the amplitude B corresponding to the degree of water adsorption in the PA chains is found to increase monotonically with RH, which will be discussed later. The exact shape of the fitted profiles clearly does not represent all features of the data, but considering the simplicity of the model with only B and I varied, and the single value of d, the representation is excellent.

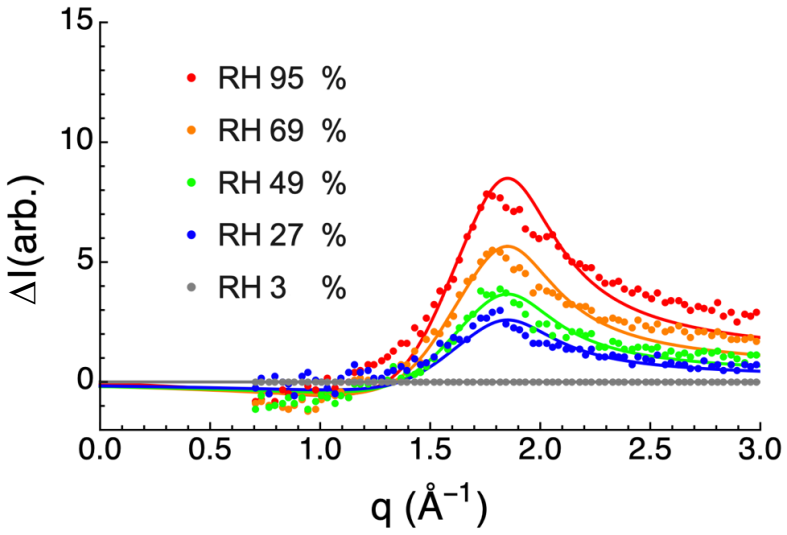

Figure 3. Fit of the circularly averaged GIWAXS profiles of a freestanding PA film at different RH values (after the subtraction of the profile at 3% RH). The fittings were achieved using the Interface Scattering Model described in Eq. (3).

To validate our chosen ϕ parameter ($\phi = 90°$) in the interface scattering model, and to confirm that there is no cross-term between the two terms corresponding to the 3.5 Å and 4.0 Å spacings, different phase factors ϕ between the two independent parts of the PA chain (with molecular spacings of 4.0 and 3.5 Å, respectively) were investigated for the best fit. The results are shown in Figure S4 (*Supporting Information*).

The ISM model provides a reasonable representation of the circularly averaged GIWAXS profiles for the PA film at different RH values with only one adjustable parameter (the amplitude B). To further test the validity of the approach, the ISM model was also used to analyze the sector

averaged GIWAXS profiles under different conditions. The 2D GIWAXS pattern from the PA film in vacuum, after the Ewald correction, is shown in Figure S3A (*Supporting Information*), where the sector averaging was obtained by integrating the intensity over ± 5° of the nominal azimuthal angle (χ). Fittings of the sector averaged GIWAXS profiles at different χ values of the dry PA film using Eq. (1) are illustrated in Figure S3B (*Supporting Information*). Overall, the fitting quality of the sector averaged GIWAXS profiles are better than that of the circularly averaged GIWAXS profiles, especially in the higher q region (> 2.0 Å^{-1}). This is understandable as the circular averaging ignored the anisotropic feature of the PA film, thus cumulating the fitting discrepancies. The modeling of the sector averaged GIWAXS profiles at different χ yielded slightly different parameters in $I,$ and r but were consistent for ϕ_1 value around 90°, and q_1 and q_2 around 1.55 Å^{-1} and 1.85 Å^{-1}, respectively. For the wet PA film, the fittings of the sector averaged GIWAXS profiles at χ = 40° ± 5° under varying RH using Eq. (3) with only one parameter (B) are illustrated in Figure S5 (*Supporting Information*), where the fits are more consistent than those in Figure 3.

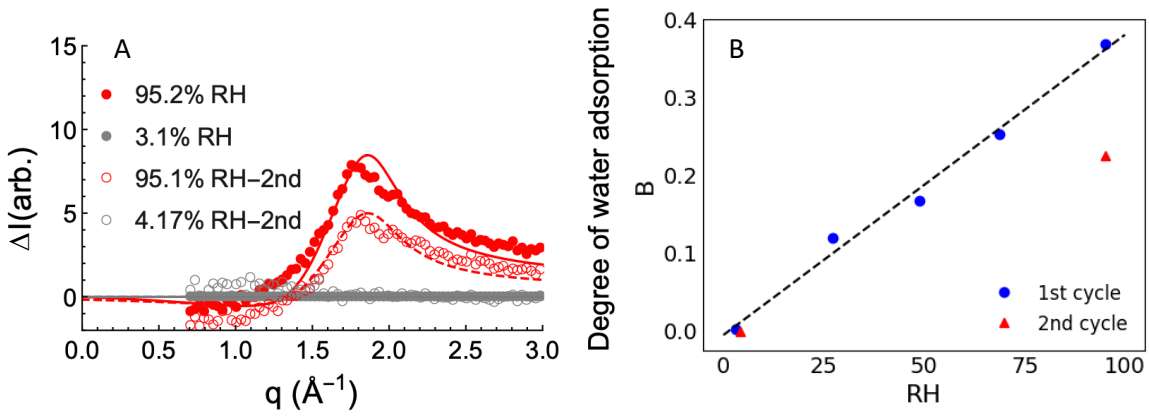

Figure 4. GIWAXS reversibility test of the PA film at varying RH. The film was tested for two humidity cycles and compared with their fitted parameters. (A) The circularly averaged GIWAXS profiles for the PA film obtained at the highest and lowest RH in the first (filled dots and solid lines) and second (open dots and dashed lines) cycles, fitted by the Interface Scattering Model. (B) Fitted degree of water adsorption as determined by parameter B is plotted against RH for the first (blue circle) and second (red triangle) cycles.

Figure 4 shows the comparison of the GIWAXS results from the PA film in the first and second humidity cycles using the Interface Scattering Model. Figure 4A illustrates the circularly averaged GIWAXS profiles obtained at the highest and lowest RH in the first and second cycles with the corresponding fits. It was found that the GIWAXS profiles in the first and second cycles agree very well at the lowest RH (3 - 4%) but exhibited some differences at the highest RH (~95%). Figure 4B provides further insight into the reversibility by comparing the fitted parameter *B* (proportional to the degree of water adsorption in the PA film) from the GIWAXS profiles at varying RH levels in both cycles. Here the dimensionless parameter *B* reflects the humidity

dependent term in Eq. 3. As shown in Figure 4B, during the first cycle the humidity parameter *B* varies in a linear manner with humidity from 0 (at the lowest humidity) to 0.37 (at the highest humidity). This observation is in contrast with the capillary condensation observed by the WAXS technique, which suggests that the interactions between the water molecules and the PA chains may be different from the phenomenon of capillary condensation.[43] In Figure 4B, the degree of water adsorption in the PA film exhibited a similar value at the lowest RH in both first and second humidity cycles, indicating the full dehydration state of the PA film. This observation agrees with our X-ray reflectivity (XR) measurement, where the results are shown in Figure S6 (*Supporting Information*). In this study, we examined the thickness expansion of a freestanding polyamide film from dry state (0% RH) to wet state (~100% RH) and then back to dry state (0% RH). The XR results indicated a 5% swelling in the z-direction, where the thickness expansion was almost fully reversible upon drying in the second cycle. However, the *B* value at the highest RH (~95%) in the second cycle did not fully return to that in the first cycle at the same RH (the final *B* value in the second cycle is similar to that found at RH between ~60% and ~80% in the first cycle). In this study, we have set the system equilibration time of 20 min before the collection of the scattering data, according to our prior time resolved GIWAXS results of PA films (thickness ~20 nm) under varying humidity. The difference in the fitted *B* values at the highest RH values in the two cycles might indicate a partial collapse of the nanopores in the PA film.

As the structure in the PA film exhibited azimuthal anisotropy, an analysis was carried out at the highest humidity (RH = ~95%) at different azimuthal angles χ using the ISM approach. The results are illustrated in Figure S7 (*Supporting Information*), which shows three selected sectoral profiles calculated from the GIWAXS pattern (after subtracting from the profile at 3% RH). In this

approach, we averaged the results over 5° of a centered azimuthal angle (χ = 10°, 40°, and 80°). In these fits, we varied *I*, *B* and *r* for the sectoral profiles at angles of 10°, 40°, and 80°, where the best fits give *r* equal to 2.75, 1.50 and 0.42, and *B* equal to 0.30, 0.29, and 0.28, respectively. It is seen that *B* does not change significantly with the azimuthal angle, but *r* does. This suggests that the adsorbed water interferes more with the first polymer term (q_1 = 1.55 Å^{-1}) than with the second polymer term (q_2 = 1.85 Å^{-1}). Sector averaged GIWAXS profiles of the three azimuthal angles (χ = 10°, 40° and 80°) by averaging over ± 5° at various RH, and their corresponding fits using the ISM are shown in Figure S8 (*Supporting Information*). The results indicate an excellent representation for χ = 40° for all RH values. However, for χ = 10°, the fitted profiles peaks are at q-values slightly higher than the experimental data, but for χ = 80°, the fitted profiles peaks are at q-values lower than the experimental data.

Atomistic MD Simulations of PA Film for Water Adsorption

To gain new insights into the atomic-scale information and the dynamics of interfacial hydration in the PA barrier layer, as well as results to support some hypotheses made in the ISM, we performed atomistic MD simulations to complement the experimental measurement. Snapshots of the MD simulations are illustrated in Figure 5. At the initial state ($t = 0$ ns), the dry PA film with 70% crosslinking degree was used, where water molecules were added in the top and bottom vacuum space (Figure 5A). Shortly after the simulation started at $t = 0.1$ ns, the water molecules absorbed onto the surface of the PA film, as shown in Figure 5B. The adsorption process was driven by strong molecular interactions between the water molecules and the subnanoporous PA

surface, including surface tension, adhesive forces, and cohesive forces (i.e., the interactions among adsorbed water molecules). As the simulation progressed, the water molecules continued to diffuse into the PA film, forming flow channels, as illustrated in Figure 5C.

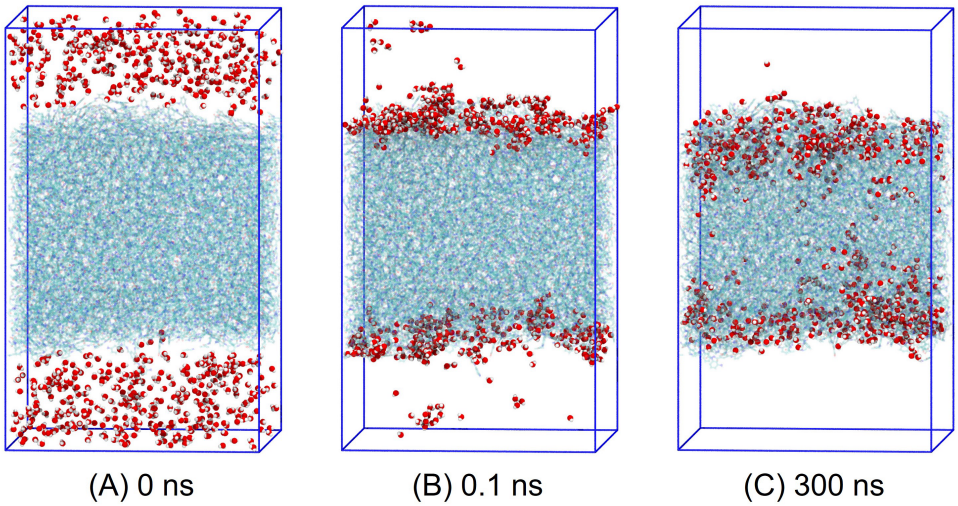

Figure 5. Snapshots of the MD simulation system. (A) At the initial state, $t = 0$ ns, the dry PA film with 70% crosslinking degree was placed in the center region, and water molecules were added in the top and bottom vacuum space; (B) At $t = 0.1$ ns, water molecules rapidly absorbed on the surface of PA film; (C) At the final state, $t = 300$ ns, water molecules diffused into the PA film due to capillary action.

The corresponding density profiles of the PA film and water along the Z-axis at varying times during the MD simulation (Figure 5) are illustrated in Figure 6. It was seen that at $t = 0$ ns, all water molecules were located outside the PA film (Figure 6A). Within 0.1 ns, almost all water molecules were attached to the surface of the PA film, as depicted in Figure 6B. By 300 ns, a small

number of the water molecules diffused into the inner region of the PA film (-25 Å < Z < 25 Å), while the majority remained on the surface area, as shown in Figure 6C. A water concentration gradient from the PA film surface to the inner membrane regions was observed for our case study after exposing the PA film to moisture (Figure 5C and Figure 6C). The results demonstrated that the entire process consists of the initial surface condensation and subsequent diffusion inside the membrane. It is noteworthy that a recent study showed that water transfer in the polyamide layer of the RO membrane is governed by the pressure gradient, which can be described by the solution-friction model.[44] Another study also demonstrated that water transfer in polyamide membranes can be described by a multimodal diffusion mechanism, consisting of localized, translational, and long-range diffusion processes.[45] However, in our system, which is in the gas phase with a dilute water concentration, the initial stage of water transfer is driven by the concentration gradient, following a solution-diffusion process (Figure 5). This is because the focus of this study is on the investigation of the initial water adsorption in a dried membrane in the transition state as well as the effect of humidity on the microstructure of the PA layer, rather than those on the steady-state molecular transport.

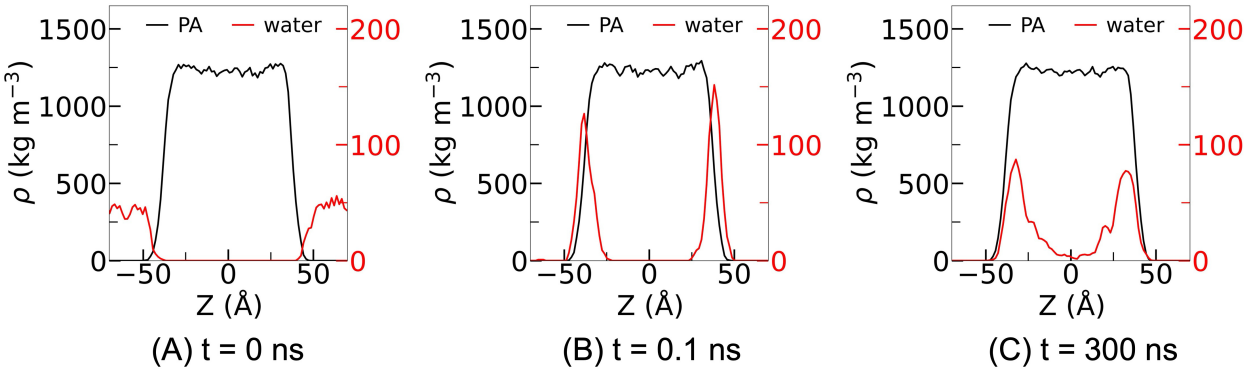

Figure 6. Density profiles of the PA film and water along the Z-axis at simulation times of (A) $t = 0$ ns, (B) $t = 0.1$ ns, and (C) $t = 300$ ns.

Figure 7 shows the radial distribution function ($g(r)$) profiles of the PA film at $t = 300$ ns, which illustrates the normalized density distribution of water molecules within the inner region of the film with respect to carboxyl oxygen (O), amino hydrogen (H), amino nitrogen (N), and benzene carbon (C) atoms of the PA chains. The $g(r)$ profiles were normalized by the average density of water molecules within the inner region. The profiles in Figure 7 clearly demonstrate that water molecules exhibit a preferential distribution around the oxygen atoms on the polymer backbone, which can be attributed to strong hydrogen bonding interactions between hydrogen atoms of the water molecules and carboxyl oxygen atoms of the PA chains. The hydrogen atoms of the amino and hydroxyl groups can also form hydrogen bonds with the oxygen atoms of the water molecules, however, the hydrogen atoms in the benzene rings can only form weak van der Waal interactions with the water molecules. A similar main peak feature is observed in the g(r) profile for the nitrogen atoms in Figure 7, but the main peak position is located at a larger radius. Due to the hydrophobic nature of the carbon atoms, very few water molecules were found in their

vicinity. The above analysis in Figure 7 indicates that water molecules are assembled around the hydrophilic groups (carboxylic acid and amine groups) of the PA chain. The distance *r* for the maximum peak in Figure 7 indicates the primary distance between the normalized density distribution of water molecules and the atoms (O/H/N/C) of the referenced polymer chain. The observed low *r* values for the maximum peaks of O, H, and N (2 - 3 Å) suggest our hypothesis that the phase factor *d* (the distance between water and the adsorption site of the PA chain) can be set to zero in the ISM analysis is reasonable.

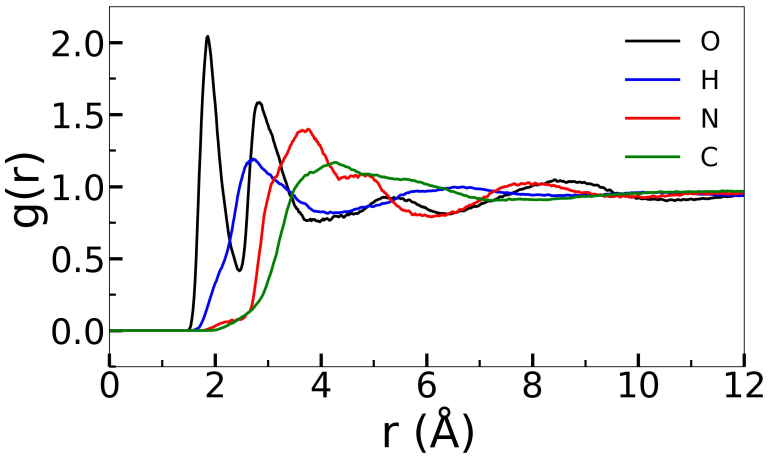

Figure 7. Radial distribution function profiles (g(r)) of water molecules in the inner area of the PA film with respect to carboxyl oxygen (O), hydrogen (H, including hydrogen atoms in amino, carboxyl, and benzene groups), amino nitrogen (N), and carbon (C).

Figure 8 shows the computed water coordination number (N_c) within the PA film, quantifying the number of neighboring water molecules surrounding a water molecule at a certain radial distance (*r*). In our prior studies, we demonstrated that only the first hydration shell exists

for water molecules within the membrane, with the second hydration shell absent.[31-32] At the cutoff distance ($r = 3.3$ Å), corresponding to the bottom of the first hydration shell, the N_c is approximately 2.8, when the polymer membrane is soaked in bulk liquid water. In this study, when the PA film was exposed to water vapor and the system reached the equilibrium state (i.e., $t = 300$ ns), N_c is only ~0.7, which indicates sparse water distribution within the polymer membrane (Figure 8A). As evidenced in Figure 8B, water molecules are isolated inside a pore forming hydrogen bonding with the PA film.

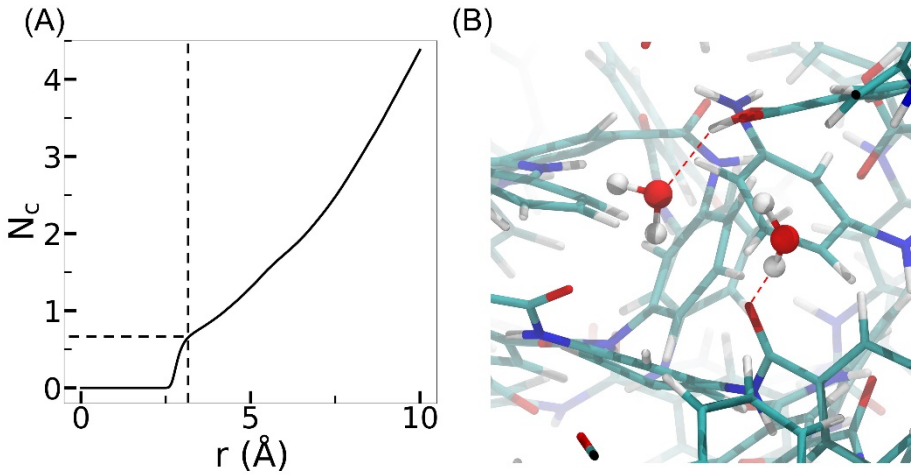

Figure 8. (A) Coordination number (N_c) of water molecules within the inner region of PA film at 300 ns. The cutoff distance of the first hydration shell ($r = 3.3$ Å) is indicated by dash lines. (B) Snapshot of water distribution at the inner area of the PA film. Hydrogen bonds are indicated with red dashed lines.

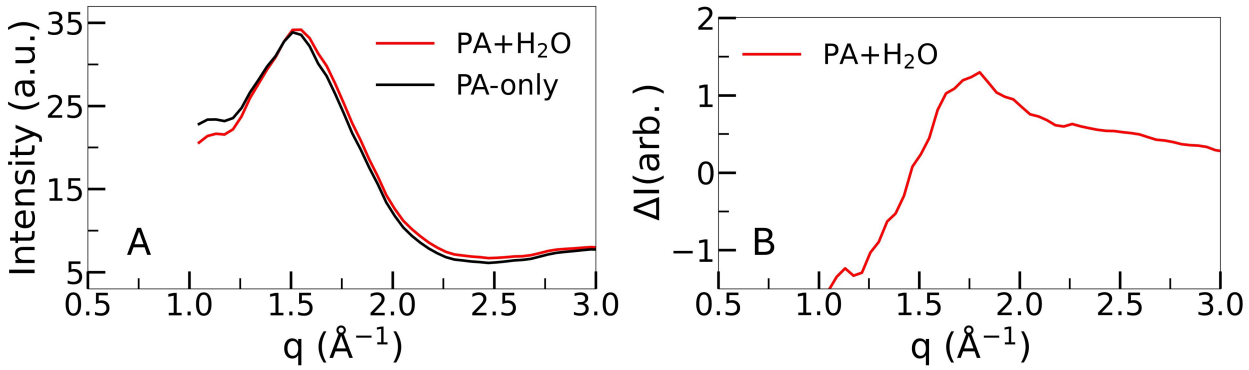

Figure 9. (A) Comparison of the scattering profiles calculated for a PA film alone and a wet PA film (including both PA and water). *(B) Difference scattering intensity profiles after subtracting the intensity values of the PA from the wet PA membrane.*

To study the influence of sparsely adsorbed water on the X-ray scattering signal, we computed the scattering profiles for a PA film alone (without including water) and for the entire system (including both PA and water) using Cromer's method.[41] The simulated scattering profile (Figure 9A) exhibited similar features to the experimental profiles (Figure 2B), even though a small simulation box was used and the content of water molecules was significantly above the experimental relative humidity. For example, both simulated and experimental scattering profiles (Figures 9C and 2C, respectively), after the background subtraction, displayed a water profile with similar feature. Specifically, the simulations showed a water peak ranging from 1.0 $Å^{-1}$ to 3.0 $Å^{-1}$, centering on $q \sim 1.85$ $Å^{-1}$, which were also observed in the experimental data (Figure 2C). Furthermore, the simulated results are consistent with the experimental findings, i.e., the presence of a small amount of adsorbed water in the dry PA film enhances the scattered intensity at the high q region and decreases the scattered intensity at the low q region (Figure 2C). The consistency

between simulation results and experimental data lends support to our observations and hypotheses derived from interface scatterings.

Conclusions

In this study, GIWAXS experiments of free-standing PA films under varying humidity were carried out to explore the intermolecular interactions of water adsorption within the polyamide scaffold. To analyze the GIWAXS results, a novel Interface Scattering Model using the phase factor between the absorbed water and surrounding PA moieties was developed. This model offers a unique and simple approach to analyze the GIWAXS profiles of the wet PA films that can quantify the water content adsorbed in the PA scaffold. Atomistic MD simulations support some aspects of the hypothesis made in the Interface Scattering Model approach. The simulation results revealed that water transport through the PA membrane comprises two steps: (1) rapid formation of a condensation layer on the PA film surface, followed by (2) slow diffusion of water molecules through the membrane. Water molecules are sparsely adsorbed in subnanopores near the polar atoms of the PA chains. These isolated water molecules do not form hydrogen bonds with neighboring water molecules. Notably, although present in low quantities, these adsorbed water molecules modify the X-ray scattering signals at high q values which are consistent with the experimental results.

Acknowledgement

The authors acknowledge the financial support from the NSF CBET's Interfacial Engineering program (CBET-2132524). NV acknowledges the support of the fellowship from an NSF NRT Award for the Quantitative Analysis of Dynamic Structures (DGE-1922639). GIWAXS experiments were carried out at the Complex Materials Scattering (CMS/11- BM) beamline at the National Synchrotron Light Source II at Brookhaven National Laboratory, funded by the U.S. DOE Office of Science Facilities under Contract DE- SC0012704. We gratefully thank Ruipeng Li and Masafumi Fukuto for support at the CMS beamline and for scientific discussions. The authors further thank Peter Beaucage and Christopher Stafford from National Institute of Standards and Technology (NIST) for discussions about conducting humidity measurements. TW and BSH are also grateful for the computational resources from the program of ACCESS (MAT230077) and the Texas Advanced Computing Center (TACC).

Supporting Information

Supplementary figures for the manuscript. Snapshots of the diluted system containing only 50 water molecules in MD simulations at varying simulation times. Density profiles of the PA film and water molecules along the Z-axis of the diluted system at varying simulation times. 2D GIWAXS patterns from the PA film in vacuum, and fittings of the sector averaged GIWAXS profiles using the interface scattering model. Fittings of circularly averaged GIWAXS profiles using the interface scattering model with different values of phase factor (ϕ). Fittings of the sector average GIWAXS profiles at the azimuthal angle $\chi = 40 \pm 5°$ from the PA film under varying RH.

X-ray reflectivity (XR) study on a freestanding PA film (thickness ~16 nm) in dry and 100% humidity conditions. Sector averaged GIWAXS profiles at ~95% RH by averaging over ± 5° of χ.

References

(1) Lau, W. J.; Ismail, A. F.; Misdan, N.; Kassim, M. A., A Recent Progress in Thin Film Composite Membrane: A Review. *Desalination* **2012,** *287*, 190-199.

(2) Fane, A. G.; Tang, C. Y.; Wang, R., Membrane Technology for Water: Microfiltration, Ultrafiltration, Nanofiltration, and Reverse Osmosis. *Treatise on Water Science* **2011,** *4*, 301-335.

(3) Cadotte, J. E.; Petersen, R. J.; Larson, R. E.; Erickson, E. E., A New Thin-Film Composite Seawater Reverse Osmosis Membrane. *Desalination* **1980,** *32*, 25-31.

(4) Freger, V., Kinetics of Film Formation by Interfacial Polycondensation. *Langmuir* **2005,** *21* (5), 1884-1894.

(5) Cadotte, J. E., Evolution of Composite Reverse Osmosis Membranes. *ACS Sym. Ser.* **1985,** *269*, 273-294.

(6) Kucera, J., *Reverse Osmosis: Industrial Processes and Applications*. John Wiley & Sons: 2015.

(7) Misdan, N.; Lau, W. J.; Ismail, A. F., Seawater Reverse Osmosis (Swro) Desalination by Thin-Film Composite Membrane—Current Development, Challenges and Future Prospects. *Desalination* **2012,** *287*, 228-237.

(8) Cadotte, J. E., Cobian, K. E., Forester, R. H., Petersen, R. J., Continued Evaluation of in-Situ-Formed Condensation Polymers for Reverse Osmosis Membranes. *National Technical Reports Library* **1976**, PB253193.

(9) Ding, M.; Szymczyk, A.; Ghoufi, A., Hydration of a Polyamide Reverse-Osmosis Membrane. *J. Membr. Sci.* **2016,** *501*, 248-253.

(10) Shen, M.; Keten, S.; Lueptow, R. M., Rejection Mechanisms for Contaminants in Polyamide Reverse Osmosis Membranes. *J. Membr. Sci.* **2016,** *509*, 36-47.

(11) Ismail, A. F.; Padaki, M.; Hilal, N.; Matsuura, T.; Lau, W. J., Thin Film Composite Membrane — Recent Development and Future Potential. *Desalination* **2015,** *356*, 140-148.

(12) Kwak, S. Y.; Jung, S. G.; Yoon, Y. S.; Ihm, D. W., Details of Surface Features in Aromatic Polyamide Reverse Osmosis Membranes Characterized by Scanning Electron and Atomic Force Microscopy. *J. Polym. Sci., Part B: Polym. Phys.* **1999,** *37* (13), 1429-1440.

(13) Yan, H.; Miao, X.; Xu, J.; Pan, G.; Zhang, Y.; Shi, Y.; Guo, M.; Liu, Y., The Porous Structure of the Fully-Aromatic Polyamide Film in Reverse Osmosis Membranes. *J. Membr. Sci.* **2015,** *475*, 504-510.

(14) Akin, O.; Temelli, F., Probing the Hydrophobicity of Commercial Reverse Osmosis Membranes Produced by Interfacial Polymerization Using Contact Angle, Xps, Ftir, Fe-Sem and Afm. *Desalination* **2011,** *278* (1-3), 387-396.

(15) Chowdhury, M. R.; Steffes, J.; Huey, B. D.; McCutcheon, J. R., 3d Printed Polyamide Membranes for Desalination. *Science* **2018,** *361* (6403), 682-686.

(16) Belfer, S.; Purinson, Y.; Fainshtein, R.; Radchenko, Y.; Kedem, O., Surface Modification of Commercial Composite Polyamide Reverse Osmosis Membranes. *J. Membr. Sci.* **1998,** *139* (2), 175-181.

(17) Zimudzi, T. J.; Feldman, K. E.; Sturnfield, J. F.; Roy, A.; Hickner, M. A.; Stafford, C. M., Quantifying Carboxylic Acid Concentration in Model Polyamide Desalination Membranes Via Fourier Transform Infrared Spectroscopy. *Macromolecules* **2018,** *51*, 6623-6629.

(18) Fujioka, T.; Oshima, N.; Suzuki, R.; Khan, S. J.; Roux, A.; Poussade, Y.; Drewes, J. E.; Nghiem, L. D., Rejection of Small and Uncharged Chemicals of Emerging Concern by Reverse Osmosis Membranes: The Role of Free Volume Space within the Active Skin Layer. *Sep. Purif. Technol.* **2013,** *116*, 426-432.

(19) Fujioka, T.; Oshima, N.; Suzuki, R.; Price, W. E.; Nghiem, L. D., Probing the Internal Structure of Reverse Osmosis Membranes by Positron Annihilation Spectroscopy: Gaining More Insight into the Transport of Water and Small Solutes. *J. Membr. Sci.* **2015,** *486*, 106-118.

(20) Fujioka, T.; O'Rourke, B. E.; Michishio, K.; Kobayashi, Y.; Oshima, N.; Kodamatani, H.; Shintani, T.; Nghiem, L. D., Transport of Small and Neutral Solutes through Reverse Osmosis Membranes: Role of Skin Layer Conformation of the Polyamide Film. *J. Membr. Sci.* **2018,** *554*, 301-308.

(21) Chu, B.; Hsiao, B. S., Small-Angle X-Ray Scattering of Polymers. *Chem. Rev.* **2001,** *101* (6), 1727-1762.

(22) Panagiotou, P.; Bauer, E.; Loi, S.; Titz, T.; Maurer, E.; Müller-Buschbaum, P., Polymeric Structures at Interfaces: An X-Ray Scattering Study. *Z. Kristallogr. Cryst. Mater.* **2004,** *219* (4), 210-217.

(23) Graewert, M. A.; Svergun, D. I., Impact and Progress in Small and Wide Angle X-Ray Scattering (Saxs and Waxs). *Curr. Opin. Struct. Biol.* **2013,** *23* (5), 748-754.

(24) Singh, P. S.; Ray, P.; Xie, Z.; Hoang, M., Synchrotron Saxs to Probe Cross-Linked Network of Polyamide 'Reverse Osmosis' and 'Nanofiltration' Membranes. *J. Membr. Sci.* **2012,** *421-422*, 51-59.

(25) Matthews, T. Growth Dynamics, Charge Density, and Structure of Polyamide Thin-Film Composite Membranes. PhD Dissertation, University of Illinois at Urbana-Champaign, 2014.

(26) Pipich, V.; Schlenstedt, K.; Dickmann, M.; Kasher, R.; Meier-Haack, J.; Hugenschmidt, C.; Petry, W.; Oren, Y.; Schwahn, D., Morphology and Porous Structure of Standalone Aromatic Polyamide Films as Used in RO Membranes – an Exploration with SANS, PALS, and SEM. *J. Membr. Sci.* **2019,** *573*, 167-176.

(27) Ridgway, H. F.; Orbell, J.; Gray, S., Molecular Simulations of Polyamide Membrane Materials Used in Desalination and Water Reuse Applications: Recent Developments and Future Prospects. *J. Membr. Sci.* **2017,** *524*, 436-448.

(28) Fu, Q.; Verma, N.; Ma, H.; Medellin-Rodriguez, F. J.; Li, R.; Fukuto, M.; Stafford, C. M.; Hsiao, B. S.; Ocko, B. M., Molecular Structure of Aromatic Reverse Osmosis Polyamide Barrier Layers. *ACS Macro Lett.* **2019,** *8* (4), 352-356.

(29) Fu, Q.; Verma, N.; Hsiao, B. S.; Medellin-Rodriguez, F.; Beaucage, P. A.; Stafford, C. M.; Ocko, B. M., X-Ray Scattering Studies of Reverse Osmosis Materials. *Synchrotron Radiat. News* **2020,** *33* (4), 40-45.

(30) Jahan Sajib, M. S.; Wei, Y.; Mishra, A.; Zhang, L.; Nomura, K.-I.; Kalia, R. K.; Vashishta, P.; Nakano, A.; Murad, S.; Wei, T., Atomistic Simulations of Biofouling and Molecular Transfer of a Cross-Linked Aromatic Polyamide Membrane for Desalination. *Langmuir* **2020,** *36* (26), 7658-7668.

(31) Wei, T.; Zhang, L.; Zhao, H.; Ma, H.; Sajib, M. S. J.; Jiang, H.; Murad, S., Aromatic Polyamide Reverse-Osmosis Membrane: An Atomistic Molecular Dynamics Simulation. *J. Phys. Chem. B* **2016,** *120* (39), 10311-10318.

(32) Zhang, C.; Bu, G.; Sajib, M. S. J.; Meng, L.; Xu, S.; Zheng, S.; Zhang, L.; Wei, T., Pxlink: A Simulation Program of Polymer Crosslinking to Study of Polyamide Membrane. *Comput. Phys. Commun.* **2023,** *291*, 108840.

(33) Karan, S.; Jiang, Z.; Livingston, A. G., Sub–10 Nm Polyamide Nanofilms with Ultrafast Solvent Transport for Molecular Separation. *Science* **2015,** *348* (6241), 1347-1351.

(34) Chan, E. P.; Lee, J.-H.; Chung, J. Y.; Stafford, C. M., An Automated Spin-Assisted Approach for Molecular Layer-by-Layer Assembly of Crosslinked Polymer Thin Films. *Rev. Sci. Instrum.* **2012,** *83* (11), 114102.

(35) Huang, H.; Zhang, C.; Crisci, R.; Lu, T.; Hung, H.-C.; Sajib, M. S. J.; Sarker, P.; Ma, J.; Wei, T.; Jiang, S.; Chen, Z., Strong Surface Hydration and Salt Resistant Mechanism of a New Nonfouling Zwitterionic Polymer Based on Protein Stabilizer Tmao. *J. Am. Chem. Soc.* **2021,** *143* (40), 16786-16795.

(36) Wei, T.; Sajib, M. S. J.; Samieegohar, M.; Ma, H.; Shing, K., Self-Assembled Monolayers of an Azobenzene Derivative on Silica and Their Interactions with Lysozyme. *Langmuir* **2015,** *31* (50), 13543-13552.

(37) Best, R. B.; Zhu, X.; Shim, J.; Lopes, P. E. M.; Mittal, J.; Feig, M.; Mackerell, A. D., Jr., Optimization of the Additive Charmm All-Atom Protein Force Field Targeting Improved Sampling of the Backbone Φ, Ψ and Side-Chain X(1) and X(2) Dihedral Angles. *J. Chem. Theory. Comput.* **2012,** *8* (9), 3257-3273.

(38) Huang, J.; Rauscher, S.; Nawrocki, G.; Ran, T.; Feig, M.; de Groot, B. L.; Grubmüller, H.; MacKerell, A. D., Jr., Charmm36m: An Improved Force Field for Folded and Intrinsically Disordered Proteins. *Nat. Methods* **2017,** *14* (1), 71-73.

(39) Darden, T.; York, D.; Pedersen, L., Particle Mesh Ewald: An N·Log(N) Method for Ewald Sums in Large Systems. *J. Chem. Phys.* **1993,** *98* (12), 10089-10092.

(40) Bussi, G.; Donadio, D.; Parrinello, M., Canonical Sampling through Velocity Rescaling. *J. Chem. Phys.* **2007,** *126* (1), 014101.

(41) Abraham, M. J.; Murtola, T.; Schulz, R.; Páll, S.; Smith, J. C.; Hess, B.; Lindahl, E., Gromacs: High Performance Molecular Simulations through Multi-Level Parallelism from Laptops to Supercomputers. *SoftwareX* **2015,** *1-2*, 19-25.

(42) László, K.; Czakkel, O.; Dobos, G.; Lodewyckx, P.; Rochas, C.; Geissler, E., Water Vapour Adsorption in Highly Porous Carbons as Seen by Small and Wide Angle X-Ray Scattering. *Carbon* **2010,** *48* (4), 1038-1048.

(43) Haynes, J. M.; McCaffery, F. G., Light Scattering and Capillary Condensation in Porous Media. *J. Colloid Interface Sci.* **1977,** *59* (1), 24-30.

(44) Wang, L.; He, J.; Heiranian, M.; Fan, H.; Song, L.; Li, Y.; Elimelech, M., Water Transport in Reverse Osmosis Membranes Is Governed by Pore Flow, Not a Solution-Diffusion Mechanism. *Sci. Adv.* **2023,** *9* (15), eadf8488.

(45) Foglia, F.; Frick, B.; Nania, M.; Livingston, A. G.; Cabral, J. T., Multimodal Confined Water Dynamics in Reverse Osmosis Polyamide Membranes. *Nat Commun* **2022,** *13* (1), 2809.